

# Exclusion of super-soft symmetry energies and neutron star properties in the saturated Nambu-Jona-Lasinio model

Si-Na Wei, Wei-Zhou Jiang, Rong-Yao Yang, Dong-Rui Zhang  
*Department of Physics, Southeast University, Nanjing 211189, China*

Considering the importance of Lorentz invariance and chiral symmetry, we adopt the Nambu-Jona-Lasinio (NJL) model that ensures the nuclear matter saturation properties to study the density dependence of the symmetry energy. The negative symmetry energy at high densities that is usually dubbed the super-soft symmetry energy can be obtained from introducing a chiral isovector-vector interaction in the lagrangian, but should be ruled out by the neutron star (NS) stability in the mean-field approximation. It is found that the isovector-scalar interaction in the NJL model can play an important role in softening of the symmetry energy. We have investigated NS properties. The NS maximum mass obtained with various isovector-scalar couplings and momentum cutoffs is well above the  $2M_{\odot}$ , and the NS radius obtained well meets the limits extracted from recent measurements. In particular, the significant reduction of the canonical NS radius occurs with the moderate decrease of the slope of the symmetry energy, while the effect of the symmetry energy on the NS maximum mass remains insignificant as usual.

PACS numbers: 11.30.Rd; 21.65.Jk; 26.60.Kp

## I. INTRODUCTION

The nuclear symmetry energy is important for understanding the reaction dynamics of heavy-ion collisions, the structures of neutron- and proton-rich nuclei, and properties of neutron stars (NS) [1–4]. Though the symmetry energy, which is the energy difference per nucleon between pure neutron matter and symmetric matter, is well constrained at saturation density to date [4–9], the density dependence of the symmetry energy is still poorly known especially at supra-normal densities [2, 10]. The symmetry energy predicted by different models is rather diverse at high densities [11–18]. Unfortunately, the symmetry energy extracted from the data with various isospin diffusion models also suffers from the large uncertainty which diversifies in super-soft [19], soft [20], and stiff [21] forms at high densities. We note that new experiments to probe the high-density symmetry energy are also on the way [22]. The super-soft symmetry energy which reaches the maximum and then turns to negative values at high densities can be obtained from some nonrelativistic models [13, 14], while the relativistic mean field (RMF) models can not produce the super-soft symmetry energy [15–18]. For instance, the nonlinear RMF models [16], the density-dependent RMF models [17, 23], and the point coupling RMF models [24–26] predict similar tendencies of symmetry energy, and no super-soft symmetry energy arises in these models [18].

The RMF models have the merit of Lorentz invariance. The success of RMF models in interpreting the pseudospin symmetry [27–29] and analyzing polarization observables in proton-nuclei reactions [30, 31] indicates that the relativistic dynamics that includes the large attractive scalar and repulsive vector is of special importance. In finite nuclei, it is the cancellation between the large scalar and vector that plays the crucial role in the structural properties. While fermions in non-relativistic models are required to be antisymmetrized, in relativistic models the fermions are indeed identified by the Dirac equation which is specifically for

fermions. It is thus not surprising that the RMF theory has achieved great success in past decades [32–42]. The merit of Lorentz invariance is also manifest in comparison with the fact that some of the non-relativistic models reach super-luminal sound speeds for high density matter at the center of neutron stars [43, 44].

As known from the QCD, the chiral symmetry serves as a cornerstone to construct the effective models of the strong interaction [45, 46]. Among many models that realize the chiral symmetry in bulk matter, e.g., see Refs. [47–51], the Nambu-Jona-Lasinio (NJL) model [47] and chiral- $\sigma$  model [48, 49] are two popular ones. The NJL model was originally proposed to realize the spontaneous symmetry breaking since the pion, as the Goldstone boson, can be derived dynamically albeit with nucleonic degrees of freedom. With the quark degrees of freedom, the NJL model is considered as an effective model for the QCD [52–54]. Since the confinement is absent in the NJL model, it is a work of art to construct the nucleons and describe nuclear matter [55]. Persisting in the character of chiral symmetry that is measured by the chiral condensate in the non-perturbative vacuum, it would be economic to realize in the NJL model the spontaneous breaking of the chiral symmetry with nucleonic degrees of freedom, like the chiral- $\sigma$  model. In this work, we thus adopt the hadron-level NJL model to check whether the covariant interactions that respect the chiral symmetry can constrain the symmetry energy. It is known that the nuclear matter saturation can not be produced by the original four-fermion interactions. The inclusion of eight-fermion interactions is important to obtain the saturation [56, 57]. This is similar to the chiral- $\sigma$  model, where the saturation is fulfilled by introducing the scalar-vector coupling [49, 58]. Similar efforts were also made to study the nuclear matter saturation and the phase diagram in the NJL model [59–61]. Note that the point coupling model is similar in form to the NJL model, and it was used to study the density dependence of the symmetry energy [18]. However, the point coupling model [24–26] was not built to manifest the

chiral symmetry that is important for the strong interaction. In order to study the density dependence of the symmetry energy, we introduce in the NJL model the isovector, isovector-vector and isovector-scalar interactions that also respect the chiral symmetry. The isovector is a four-fermion interaction, and isovector-vector and isovector-scalar terms represent the eight-fermion interaction in the NJL model. Through the isovector-vector interaction, the super-soft symmetry energy may be produced. However, we will explain why the symmetry energy in the RMF approximation can not be super-soft according to the NS stability. Moreover, we will examine how the symmetry energy evolves with the density in the NJL model.

Recently, remarkable progresses in NS observations have been achieved. Accurate mass measurements determined two large-mass NS's: the radio pulsar J1614-2230 with mass of  $M = 1.97 \pm 0.04 M_\odot$  [62] and the J0348+0432 with mass of  $M = 2.01 \pm 0.04 M_\odot$  [63]. However, there is no consensus on the extracted NS radius [64] reported in the literature [65–71], due to the systematic uncertainties involved in the distance measurements and theoretical analyses of the light spectrum [72–75]. In this work, we will thus investigate whether the parametrizations of the present saturated NJL model can satisfy the NS mass constraint and provide some useful comparisons with various NS radius constraints. In the following, we will in turn present the formalism, analyze the results, and give the summary.

## II. FORMALISM

The original NJL model that only contains scalar, pseudoscalar, vector and axial vector interactions can not reproduce saturation properties of nuclear matter. In order to obtain the saturation property, the scalar-vector (SV) interaction, which also respects the chiral symmetry, was introduced [56, 57]. The Lagrangian of the saturated NJL model can be written as [57]:

$$\begin{aligned} \mathcal{L}_0 = & \bar{\psi}(i\gamma_\mu \partial^\mu - m_0)\psi + \frac{G_S}{2}[(\bar{\psi}\psi)^2 - (\bar{\psi}\gamma_5\tau\psi)^2] \\ & - \frac{G_V}{2}[(\bar{\psi}\gamma_\mu\psi)^2 + (\bar{\psi}\gamma_\mu\gamma_5\psi)^2] \\ & + \frac{G_{SV}}{2}[(\bar{\psi}\psi)^2 - (\bar{\psi}\gamma_5\tau\psi)^2] \\ & \cdot [(\bar{\psi}\gamma_\mu\psi)^2 + (\bar{\psi}\gamma_\mu\gamma_5\psi)^2], \end{aligned} \quad (1)$$

where  $m_0$  is the bare nucleon mass.  $G_S$ ,  $G_V$  and  $G_{SV}$  are the scalar, vector and scalar-vector coupling constants, respectively. It is easy to see that the Lagrangian is chiral symmetric when  $m_0 = 0$ . In order to investigate the density dependence of the symmetry energy, we introduce the isovector, isovector-vector and isovector-scalar interactions in the Lagrangian which are written

as:

$$\begin{aligned} \mathcal{L}_{IV} = & \frac{G_\rho}{2}[(\bar{\psi}\gamma_\mu\tau\psi)^2 + (\bar{\psi}\gamma_\mu\gamma_5\tau\psi)^2] \\ & + \frac{G_{\rho V}}{2}[(\bar{\psi}\gamma_\mu\tau\psi)^2 + (\bar{\psi}\gamma_\mu\gamma_5\tau\psi)^2] \cdot \\ & [(\bar{\psi}\gamma_\mu\psi)^2 + (\bar{\psi}\gamma_\mu\gamma_5\psi)^2] \\ & + \frac{G_{\rho S}}{2}[(\bar{\psi}\gamma_\mu\tau\psi)^2 + (\bar{\psi}\gamma_\mu\gamma_5\tau\psi)^2] \cdot \\ & [(\bar{\psi}\psi)^2 - (\bar{\psi}\gamma_5\tau\psi)^2], \end{aligned} \quad (2)$$

where  $G_\rho$ ,  $G_{\rho V}$  and  $G_{\rho S}$  are the isovector, isovector-vector and isovector-scalar coupling constants, respectively.  $\mathcal{L}_{IV}$  is also chirally symmetric. Using the mean-field approximation,

$$\begin{aligned} (\bar{\psi}A\psi)(\bar{\psi}B\psi) = & (\bar{\psi}A\psi) \langle \bar{\psi}B\psi \rangle + \langle \bar{\psi}A\psi \rangle (\bar{\psi}B\psi) \\ & - \langle \bar{\psi}A\psi \rangle \langle \bar{\psi}B\psi \rangle \end{aligned} \quad (3)$$

the Lagrangian can be simplified to be

$$\begin{aligned} \mathcal{L} = & \mathcal{L}_0 + \mathcal{L}_{IV} = \bar{\psi}[i\gamma_\mu \partial^\mu - m(\rho, \rho_S) - \\ & \gamma^0 \Sigma(\rho, \rho_S, \rho_3)]\psi - U(\rho, \rho_S, \rho_3), \end{aligned} \quad (4)$$

where  $m$ ,  $\Sigma$  and  $U$  are defined as

$$m(\rho, \rho_S) = m_0 - (G_S + G_{SV}\rho^2 + G_{\rho S}\rho_3^2)\rho_S, \quad (5)$$

$$\begin{aligned} \Sigma(\rho, \rho_S, \rho_3) = & G_V\rho + G_{\rho}\rho_3\tau_3 - G_{SV}\rho_S^2\rho - G_{\rho V}\rho_3^2\rho \\ & - G_{\rho V}\rho_3\rho^2\tau_3 - G_{\rho S}\rho_3\rho_S^2\tau_3, \end{aligned} \quad (6)$$

$$\begin{aligned} U(\rho, \rho_S, \rho_3) = & \frac{1}{2}(G_S\rho_S^2 - G_V\rho^2 - G_{\rho}\rho_3^2 + 3G_{SV}\rho_S^2\rho^2 \\ & + 3G_{\rho V}\rho_3^2\rho^2 + 3G_{\rho S}\rho_3^2\rho_S^2). \end{aligned} \quad (7)$$

Eq.(5) is the gap equation for the nucleon effective mass in the NJL model. Here  $\rho = \langle \bar{\psi}\gamma^0\psi \rangle$ ,  $\rho_3 = \langle \bar{\psi}\gamma^0\tau_3\psi \rangle$  and  $\rho_S = \langle \bar{\psi}\psi \rangle$  are vector, isovector and scalar densities, respectively

$$\rho = \sum_{i=p,n} \nu_i \int_0^{p_{Fi}} \frac{d^3p}{(2\pi)^3}, \quad \rho_3 = \rho_p - \rho_n, \quad (8)$$

$$\rho_S = - \sum_{i=p,n} \nu_i \int_{p_{Fi}}^\Lambda \frac{d^3p}{(2\pi)^3} \frac{m}{\sqrt{p^2 + m^2}}, \quad (9)$$

where  $\nu_i$  is the spin degeneracy, and  $\Lambda$  is the momentum cutoff. From the energy-momentum tensor, we may obtain the expression of the energy density

$$\begin{aligned} \epsilon = & - \sum_{i=p,n} \nu_i \int_{p_{Fi}}^\Lambda \frac{d^3p}{(2\pi)^3} (p^2 + m^2)^{1/2} + \frac{G_V\rho^2}{2} \\ & + \frac{G_\rho\rho_3^2}{2} + \frac{G_S\rho_S^2}{2} + \frac{G_{SV}\rho^2\rho_S^2}{2} \\ & - \frac{G_{\rho V}\rho_3^2\rho^2}{2} + \frac{G_{\rho S}\rho_3^2\rho_S^2}{2} + \epsilon_0, \end{aligned} \quad (10)$$

where the  $\epsilon_0$ , introduced to give the vanishing energy density of the vacuum state, is given as

$$\epsilon_0 = \sum_{i=p,n} \nu_i \int_0^\Lambda \frac{d^3p}{(2\pi)^3} (p^2 + m_N^2)^{1/2} - \frac{(m_N - m_0)^2}{2G_S},$$

with  $m_N$  the nucleon mass in the free space. The pressure can be obtained from the thermodynamic relation

$$P = \sum_{i=p,n} \mu_i \rho_i - \epsilon, \mu_i = \frac{d\epsilon}{d\rho_i}, \quad (11)$$

and it is given explicitly as

$$P = - \sum_{i=p,n} \frac{\nu_i}{3} \int_{p_{F_i}}^{\Lambda} \frac{d^3k}{(2\pi)^3} \frac{k^2}{\sqrt{k^2 + m^2}} + \frac{G_V \rho^2}{2} + \frac{G_\rho \rho_3^2}{2} - \frac{G_S \rho_S^2}{2} - \frac{3G_{SV} \rho_S^2 \rho^2}{2} - \frac{3G_{\rho V} \rho_3^2 \rho^2}{2} - \frac{3G_{\rho S} \rho_3^2 \rho_S^2}{2} - \frac{2\Lambda^3 \sqrt{\Lambda^2 + m^2}}{3\pi^2} - \epsilon_0. \quad (12)$$

From the energy density, we can derive the symmetry energy as

$$E_{sym}(\rho) = \frac{1}{2} \frac{\partial^2(\epsilon/\rho)}{\partial \delta^2} \Big|_{\delta=0} = \frac{p_F^2}{6E_F} + \frac{1}{2} G_\rho \rho - \frac{1}{2} G_{\rho V} \rho^3 - \frac{1}{2} G_{\rho S} \rho_S^2 \rho, \quad (13)$$

where  $\delta = (\rho_n - \rho_p)/\rho$  is the isospin asymmetry parameter and  $E_F = \sqrt{p_F^2 + m^2}$ . For the detail of the derivation, see Appendix A. The symmetry energy has a term linear in  $\rho^3$  due to the isovector-vector interaction. The slope of the symmetry energy at saturation density is defined as

$$L = 3\rho_0 \frac{\partial E_{sym}}{\partial \rho} \Big|_{\rho_0}. \quad (14)$$

In this work, we consider the simplest compositions for NS matter: neutrons, protons and electrons. The NS composition can be obtained from solving the gap equation (5) and the conditions of chemical equilibrium and charge neutrality

$$\mu_p = \mu_n + \mu_e, \quad \rho_p = \rho_e. \quad (15)$$

### III. RESULTS AND DISCUSSIONS

The present model has eight parameters:  $\Lambda$ ,  $m_0$ ,  $G_S$ ,  $G_V$ ,  $G_{SV}$ ,  $G_\rho$ ,  $G_{\rho V}$ , and  $G_{\rho S}$ . It was pointed out in Ref. [57] that  $\Lambda > 0.6 \text{ GeV}$  should be excluded, because otherwise the bare nucleon mass  $m_0$  would be smaller than  $3m_{0q}$ , where  $m_{0q} = (5 \pm 1) \text{ MeV}$  [76] is the isospin-averaged current mass of light quarks. Indeed, the cutoff larger than 600 MeV (with  $m_0 < 3m_{0q}$ ) declines a monotonous decrease of the nucleon mass with the increase of density [57], thus disfavoring the characterization of the in-medium chiral symmetry restoration. Here, the link between the bare nucleon mass and the current quark mass can be understood upon the constituent quark picture where the current quarks are released out after the chiral symmetry is restored. Following Ref. [57], we choose  $\Lambda = 400 \text{ MeV}$  unless otherwise indicated. Using Eq.(5) and  $m_\pi^2 f_\pi^2 = m_0 \rho_S^{\text{vac}}$ , we obtain  $m_0 = 41.3 \text{ MeV}$  and  $G_S = 1.669 \text{ GeV} \cdot \text{fm}^3$ .

The saturation requirement,  $(\epsilon/\rho)_{\rho=\rho_0} - m = 16 \text{ MeV}$  with  $\rho_0 = 0.16 \text{ fm}^{-3}$  in this work, gives  $G_V = 1.581 \text{ GeV} \cdot \text{fm}^3$  and  $G_{SV} = 2.054 \text{ GeV} \cdot \text{fm}^9$ . The coupling constants  $G_{\rho V}$  and  $G_{\rho S}$  are taken as adjustable parameters to simulate different nuclear symmetry energies. For vanishing  $G_{\rho V}$  and  $G_{\rho S}$ , we obtain  $G_\rho$  to be  $0.193 \text{ GeV} \cdot \text{fm}^3$  by fitting the symmetry energy at saturation density to be  $31.6 \text{ MeV}$  [5].

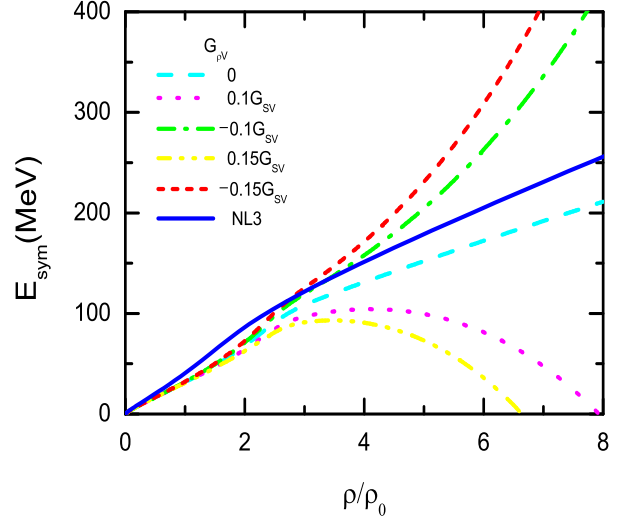


FIG. 1: (Color online) The symmetry energy for different  $G_{\rho V}$  as a function of density. Here,  $G_{\rho S}$  is set to be zero. The symmetry energy with the RMF model NL3 is also depicted for comparison.

Fig. 1 shows the symmetry energy for different  $G_{\rho V}$ . For comparison, we also depict the symmetry energy with the nonlinear RMF model NL3 [77]. We can see that the symmetry energy without the isovector-vector interaction is softer than that with the NL3, while both evolve similarly with the density. By adjusting the parameter  $G_{\rho V}$ , we can simulate various density profiles of the symmetry energy that were reported in the model predictions [14, 15] and data extractions [19–21]. Since the isovector-vector interaction contributes the symmetry energy a term that is cubic in density, as seen in Eq.(13), the modification to the symmetry energy is decisive at high densities. The symmetry energy rises stiffly for negative  $G_{\rho V}$ , while it becomes super-soft till to below zero at high densities for positive  $G_{\rho V}$ .

Now, we investigate in NS matter the consequence of the symmetry energy with various isovector-vector couplings. Firstly, we check the ratio of protons to neutrons, which is shown in Fig. 2. The ratio of protons to neutrons turns out to be very sensitive to the isovector-vector couplings, similar to the variation of the symmetry energy. The reason for this similarity lies in the fact that the difference between the proton and neutron chemical potentials, associated with the proton fraction, is linear in the symmetry energy. For negative  $G_{\rho V}$ , the proton fraction increases with the increase of density, while for positive  $G_{\rho V}$  it first increases up to a maximum and then reduces with the increase of density. Corresponding to the super-soft symmetry energy with  $G_{\rho V} = 0.1G_{SV}$  and  $0.15G_{SV}$ , the proton fraction tends

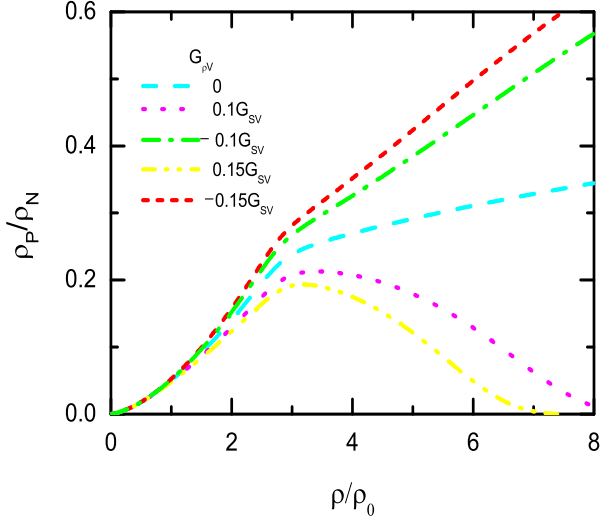


FIG. 2: (Color online) The ratio of protons to neutrons in NS matter as a function of density for various  $G_{\rho V}$ .

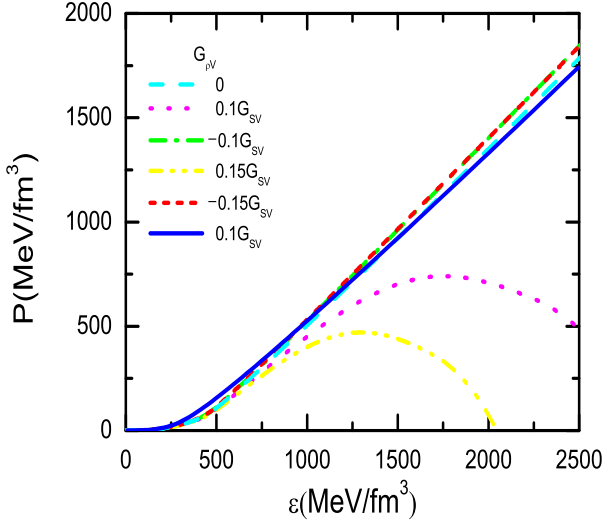


FIG. 3: (Color online) EOS's of NS matter for various  $G_{\rho V}$ .

to disappear at high densities, which means that in the NS interior pure neutron matter arises [78, 79]. As the proton fraction reduces to zero, the  $\rho^2 \rho_3^2$  term becomes proportional to  $\rho^4$ . As a result, the pressure reduces dramatically at high densities, as shown in Fig. 3. The isovector-scalar interaction with the appropriate sign of  $G_{\rho S}$  may produce some cancelation against the dramatic decrease of the pressure caused by the isovector-vector interaction. Such a cancelation is, however, almost negligible because of very small  $\rho_S$  at high densities. In this way, the EOS with the super-soft symmetry energy in the NJL model can not stabilize the NS. In non-relativistic models, the negative symmetry energies may be excluded by the stability arguments against the formation of an isospin separated phase [43, 80]. The similar NS stability problem was also found using the nonrelativistic models with the MDI interactions [81]. While the over-reduced pressure was compensated by invoking the weakly interacting light U-boson [81], such

a compensation would actually not help much in the present case because the isovector-vector interaction reduces the pressure in a form linear in  $\rho^4$ . Therefore, the super-soft symmetry energy should be excluded affirmatively in the NJL model where the interactions are constrained by the Lorentz invariance and chiral symmetry. We would, however, say that the present conclusion does not have to be universal to other approaches that account for high-order residual interactions. For instance, in the presence of the super-soft symmetry energy, the pressure of neutron star matter may increase with the density in a non-relativistic microscopic calculation with the variational method [78].

Apart from the results with negative  $G_{\rho V}$ 's in Figs. 1 and 2, we find that there is no significant difference in the pressure at high densities, as shown Fig. 3. This occurs because the  $G_{\rho V} \rho_3^2$  is much smaller than  $G_V$  for the increasing proton fraction with the density, see Eq. (12). Thus, the isovector-vector interaction just provides a minor contribution to the pressure in this case, as seen in Eq. (12). In any case, the contribution from the isovector-vector interaction is negligible at low densities. In the following we neglect the isovector-vector interaction in the calculation.

Currently, the different extraction of the slope of the symmetry energy gives an average around  $L \sim 40 - 60 \text{ MeV}$  [4–9]. With  $\Lambda = 400 \text{ MeV}$ ,  $L$  is  $93.6 \text{ MeV}$ . To reduce the slope parameter, we can not simply adjust the cutoff or the coupling constant  $G_\rho$ . A feasible way is to employ the isovector-scalar interaction. Shown in the upper panel of Fig. 4 is the symmetry energy with various isovector-scalar couplings. Here, the symmetry energy at saturation density is fixed to be  $31.6 \text{ MeV}$  by adjusting the parameter  $G_\rho$ , and  $G_\rho$  is  $0.060, 0.126, 0.260$  and  $0.326 \text{ GeV} \cdot \text{fm}^3$  for  $G_{\rho S}/G_{SV} = -0.50, -0.25, 0.25$ , and  $0.50$ , respectively. We see that the slope parameter can be reduced significantly by decreasing the  $G_{\rho S}$ . With  $G_{\rho S} = -0.5G_{SV}$ , the slope parameter is  $61.7 \text{ MeV}$ , being very close to the average of extracted values.

In above, we use the momentum cutoff  $\Lambda = 400 \text{ MeV}$ . It is significant to examine how the results change with the cutoff. When the Fermi momentum is close to and then exceeds the cutoff, we find that the chiral symmetry is nearly restored, and the scalar density and the nucleon effective mass become vanishing smoothly. In the lower panel of Fig. 4, we display the symmetry energy with various cutoffs at  $G_{\rho S} = -0.25G_{SV}$ . For various cutoffs, the parameter sets that maintain the saturation at  $\rho_0 = 0.16 \text{ fm}^{-3}$  are tabulated in Table. I. As seen from the lower panel of Fig. 4, the symmetry energy with different cutoffs may be close at high densities. The reason for this to occur is that the  $G_\rho$ , determined by the symmetry energy at saturation density, is close for different cutoffs, see Table I. At high densities, the term of  $G_\rho$  dominates the symmetry energy (see Eq. (13)), since the nucleon mass and scalar density are small for the restoration of chiral symmetry. It is interesting to see that the soft symmetry energy (at high densities) is not above the stiff one at lower densities, different from those in the literature,

TABLE I: Parameter sets for various cutoffs with  $G_{\rho S} = -0.25G_{SV}$ . Listed in the last column is the incompressibility coefficient of symmetric matter at saturation density.

$\Lambda(\text{MeV})$	$G_S(\text{GeV}\cdot\text{fm}^3)$	$m_0(\text{MeV})$	$G_{SV}(\text{GeV}\cdot\text{fm}^9)$	$G_V(\text{GeV}\cdot\text{fm}^3)$	$G_\rho(\text{GeV}\cdot\text{fm}^3)$	$G_{\rho S}(\text{GeV}\cdot\text{fm}^9)$	$\kappa(\text{MeV})$
300	3.637	95.7	2.273	3.226	0.040	-0.568	767
350	2.409	60.9	3.482	2.173	0.122	-0.871	262
400	1.669	41.3	2.054	1.581	0.126	-0.514	296
500	0.896	21.7	0.879	1.156	0.068	-0.289	315

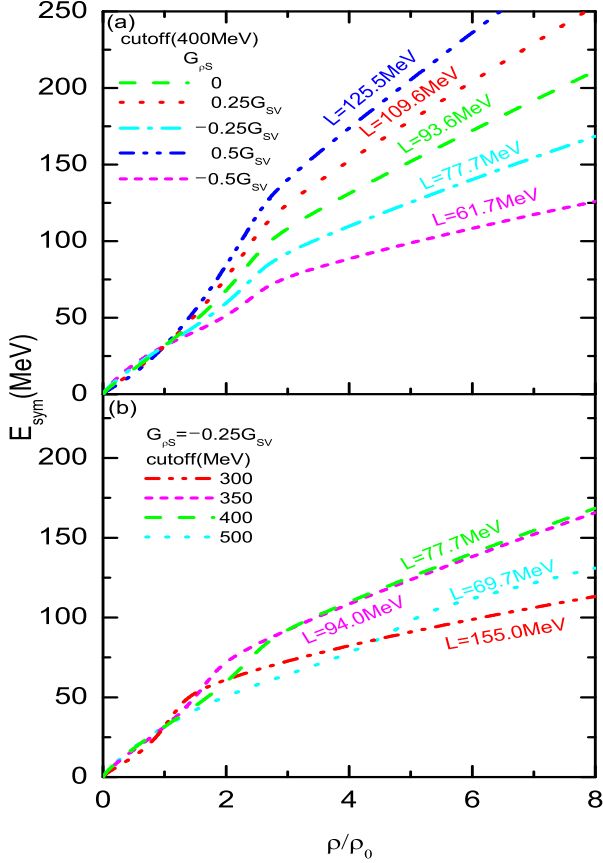


FIG. 4: (Color online) The symmetry energy with various isovector-scalar couplings (upper panel) at  $\Lambda = 400\text{MeV}$  and various cutoffs at  $G_{\rho S} = -0.25G_{SV}$  (lower panel).

e.g., see Ref. [14, 17]. We may attribute this to the behavior of the effective nucleon mass in the NJL model: there is a turning point because of the disappearance of the integration at  $p_F = \Lambda$ , see Eqs (5) and (8). With the increase of the cutoff, the turning density rises, and the similar tendency of the symmetry energy below and above saturation density still exists but fades away. However, for the fixed cutoff, the consistent softening of the symmetry energy at lower and high densities does not appear, as shown in the upper panel of Fig. 4.

Now, we turn to the NS properties with the EOS obtained in the NJL model. The mass-radius relation of NS's can be obtained by solving the standard Tolman-Oppenheimer-Volkoff (TOV) equation [82, 83]. We adopt the EOS's obtained in this work at densities above half the saturation density, while since

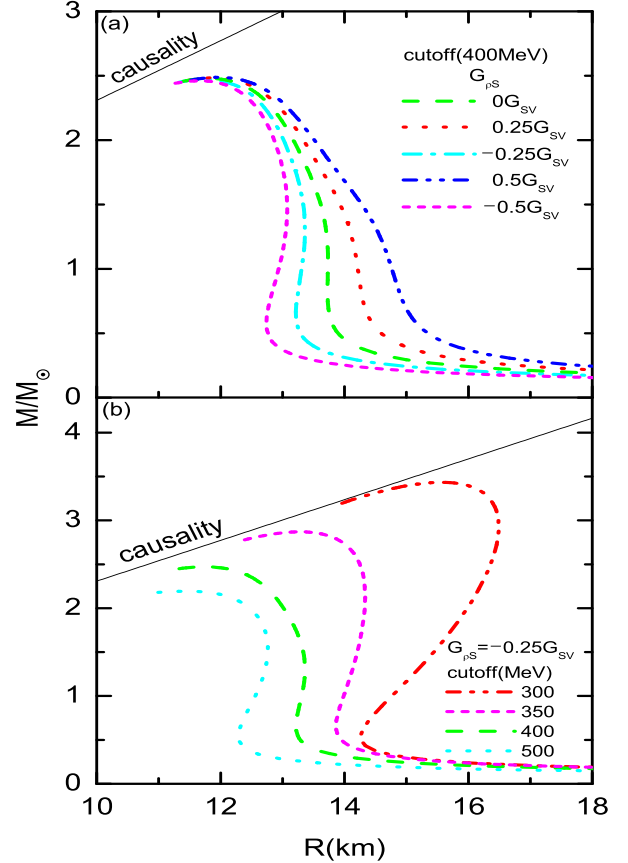


FIG. 5: (Color online) The same as in Fig. 4 but for NS mass-radius trajectories.

at lower densities NS matter transitions to inhomogeneous phase, we employ the standard low-density EOS [84, 85]. A detailed treatment of the core-crust transition can give a transition density different from half the saturation density [86]. It is, however, found in our calculations that the small difference in the transition density does not have visible effects on the NS radii. Shown in Fig. 5 are NS mass-radius relations with the cases same as in Fig. 4. We see all cases can give rise to the NS maximum mass larger than  $2M_\odot$ , satisfying the maximum mass constraint [62, 63]. With the given cutoff, the isovector-scalar interaction does not have significant effects on the high-density EOS since the scalar density and nucleon effective mass are small at high densities. Thus, the NS maximum mass that is dominated by the high-density EOS does not change much by the isovector-scalar coupling, as seen in the



upper panel of Fig. 5. While the NS radius is primarily determined by the slope of the symmetry energy in the density range of 1 to  $2\rho_0$  [87, 88], the different  $L$ , shown in the upper panel of Fig. 4, can account for the large extent of different NS radii. The radius of a canonical NS without the isovector-scalar coupling is about 13.7 km, locating at a reasonable position among various predictions [17, 87, 89] and extractions from recent observations [66–71] ranging roughly from 10 to 15 km. With decreasing the isovector-scalar coupling, the NS radius reduces accordingly. For instance, with  $G_{\rho S} = -0.5G_{SV}$ , the radius of the  $1.4M_\odot$  NS is decreased to be 13 km, which is the same as the lower limit extracted from the observation of 4U 1608-52 [68].

Shown in the lower panel of Fig. 5 is the mass-radius relation for various cutoffs at  $G_{\rho S} = -0.25G_{SV}$ . We see that the NS maximum mass is significantly larger for smaller cutoffs. This is attributed to the stiffening of the high-density EOS by decreasing the cutoff. Since the scalar density that determines the nucleon effective mass is small at high densities, the vector term, denoted by the coupling  $G_V$ , matters the stiffness of the EOS at high densities greatly. While the vector coupling constant is larger for smaller cutoffs, see Table I, the EOS becomes stiffer with the decrease of the cutoff, resulting in larger NS maximum mass. Remarkably, the NS maximum mass can reach about  $2.85 M_\odot$  for the parameter set with  $\Lambda = 350 \text{ MeV}$  that predicts a very reasonable incompressibility for symmetric matter. It is interesting to see that the NS radius decreases significantly with the increase of the cutoff. Similar to the case with various isovector-scalar couplings, the decrease of NS radius is associated with the slope parameter  $L$ . The  $L$  is 155.0, 94.0, 77.7, and 69.7 MeV with the cutoff 300, 350, 400 and 500 MeV, respectively. This is roughly corresponding to different NS radii, as shown in the lower panel of Fig. 5. We should, however, note that different cutoffs can result in the difference in properties of symmetric matter that also contribute to the large separation in NS radii. For instance, rather different incompressibility at saturation density arises for various cutoffs, as seen in Table I. Recently, it has been a hot topic, albeit controversial, whether there exists the NS with small radius, e.g., see Refs. [64, 72]. Our investigation indicates that a suitable combination of the cutoffs and isovector-scalar couplings in the saturated NJL model can favorably lead to relatively small NS radii which are consistent with those extracted from recent measurements [66–71]. We may reasonably require the positive  $G_\rho$  at any  $G_{\rho S}$  to fit the symmetry energy at saturation density. Within the cutoff range of 300–500 MeV for non-positive  $G_{\rho S}$ , we can estimate the radius region of the  $1.4M_\odot$  NS to be around 12.5–15.5 km.

#### IV. SUMMARY

In this work, we adopt the saturated NJL model that respects the chiral symmetry and Lorentz invariance to study the density dependence of the symmetry energy and its consequence in NS's. While the super-soft sym-

metry energy can not be produced by the usual RMF models, we introduce a chiral isovector-vector interaction to simulate the super-soft symmetry energy. We have found that isovector-vector interaction contributes a  $\rho^3$  term to the symmetry energy, and the symmetry energy can be super-soft or stiff, depending on the sign of isovector-vector interaction. However, with the super-soft symmetry energy, the NS matter pressure decreases at high densities and fails to keep NS stable. Thus, the super-soft symmetry energy should be ruled out by the observation of stable NS's. It is found that the isovector-scalar interaction in the NJL model plays an important role in softening of the symmetry energy. We have also examined the dependence of the symmetry energy on the momentum cutoff of the NJL model. The rise of the cutoff in a reasonable region reduces the slope of the symmetry energy at saturation density. For smaller cutoffs, the symmetry energy in the NJL model may display consistent stiffness or softness on the both sides of the saturation density. Finally, using the NJL EOS's, we have investigated the NS mass-radius relations. The NS maximum mass obtained with various isovector-scalar couplings and momentum cutoffs is well above the  $2M_\odot$ . The relatively small NS radius can be obtained with suitable combination of reasonable cutoffs and isovector-scalar couplings, and the obtained NS radii well meet the present limits extracted from recent measurements.

#### ACKNOWLEDGMENT

We thank Profs. Lie-Wen Chen and Hong-Shi Zong for helpful discussions. The work was supported in part by the National Natural Science Foundation of China under Grant No. 11275048 and the China Jiangsu Provincial Natural Science Foundation under Grant No. BK20131286.

#### Appendix A: Derivation for the symmetry energy

The symmetry energy can be obtained from the second derivative of the energy per nucleon, see Eq.(13). Here, we use a simple energy density

$$\epsilon = - \sum_{i=p,n} \nu_i \int_{p_{Fi}}^{\Lambda} \frac{d^3p}{(2\pi)^3} (p^2 + m^2)^{1/2} + \frac{G_S \rho_S^2}{2} + \frac{G_{SV} \rho^2 \rho_S^2}{2} + \frac{G_{\rho S} \rho_3^2 \rho_S^2}{2}, \quad (\text{A1})$$

to give the derivation. By defining the energy per nucleon

$$f(\rho, \delta) = \epsilon / \rho, \quad (\text{A2})$$

and using the variables  $(\rho_p, \rho_n)$ ,

$$\rho_p = \rho_p(\rho, \delta), \quad \rho_n = \rho_n(\rho, \delta), \quad (\text{A3})$$

we can write in turn the first and second derivatives of  $f$  with respect to  $\delta$ ,

$$\frac{\partial f}{\partial \delta} = \frac{\partial f}{\partial \rho_n} \frac{\partial \rho_n}{\partial \delta} + \frac{\partial f}{\partial \rho_p} \frac{\partial \rho_p}{\partial \delta}, \quad (\text{A4})$$

$$\frac{\partial^2 f}{\partial \delta^2} = \frac{\partial}{\partial \delta} \left( \frac{\partial f}{\partial \rho_n} \frac{\partial \rho_n}{\partial \delta} + \frac{\partial f}{\partial \rho_p} \frac{\partial \rho_p}{\partial \delta} \right). \quad (\text{A5})$$

As an example, we write down here the derivative over the neutron density  $\rho_n$  explicitly

$$\begin{aligned} \frac{\partial f}{\partial \rho_n} = & \sum_{i=p,n} \frac{\nu_i}{\rho^2} \int_{p_{Fi}}^{\Lambda} \frac{d^3 p}{(2\pi)^3} \sqrt{p^2 + m^2} + \sqrt{p_{Fi}^2 + m^2} / \rho \\ & - \sum_{i=p,n} \frac{\nu_i}{\rho} \int_{p_{Fi}}^{\Lambda} \frac{d^3 p}{(2\pi)^3} \frac{m}{\sqrt{p^2 + m^2}} \frac{\partial m}{\partial \rho_n} - \frac{G_S \rho_S^2}{2\rho^2} \\ & + \frac{G_S}{\rho} \frac{\rho_S}{\rho} \frac{\partial \rho_S}{\partial \rho_n} + \frac{G_{SV} \rho_S^2}{2} + G_{SV} \rho \rho_S \frac{\partial \rho_S}{\partial \rho_n} \\ & - \frac{G_{\rho S} \rho_3^2 \rho_S^2}{2\rho^2} - \frac{G_{\rho S} \rho_3 \rho_S^2}{\rho} + \frac{G_{\rho S} \rho_3^2 \rho_S}{\rho} \frac{\partial \rho_S}{\partial \rho_n}. \quad (\text{A6}) \end{aligned}$$

Using the gap equation, we obtain the relation for  $\partial m / \partial \rho_n$

$$\begin{aligned} \frac{\rho_S}{\rho} \frac{\partial m}{\partial \rho_n} = & - \frac{G_S \rho_S}{\rho} \frac{\partial \rho_S}{\partial \rho_n} - 2G_{SV} \rho_S^2 - G_{SV} \rho \rho_S \frac{\partial \rho_S}{\partial \rho_n} \\ & + \frac{2G_{\rho S} \rho_3 \rho_S^2}{\rho} - \frac{G_{\rho S} \rho_3^2 \rho_S}{\rho} \frac{\partial \rho_S}{\partial \rho_n}. \quad (\text{A7}) \end{aligned}$$

Eventually, the first and second derivatives of  $f$  with respect to  $\delta$  are given as

$$\frac{\partial f}{\partial \delta} = \frac{\sqrt{p_{Fn}^2 + m^2}}{2} - \frac{\sqrt{p_{Fp}^2 + m^2}}{2} + G_{\rho S} \rho_3 \rho_S^2 \quad (\text{A8})$$

$$\begin{aligned} \frac{\partial^2 f}{\partial \delta^2} = & \frac{\rho \pi^2}{4p_{Fn} \sqrt{p_{Fn}^2 + m^2}} + \frac{\rho \pi^2}{4p_{Fp} \sqrt{p_{Fp}^2 + m^2}} \\ & + \frac{\rho m}{4} \left( \frac{1}{\sqrt{p_{Fn}^2 + m^2}} - \frac{1}{\sqrt{p_{Fp}^2 + m^2}} \right) \times \\ & \left( \frac{\partial m}{\partial \rho_p} - \frac{\partial m}{\partial \rho_n} \right) + G_{\rho S} \rho \rho_3 \rho_S \frac{\partial \rho_S}{\partial \rho_n} \\ & - G_{\rho S} \rho \rho_3 \rho_S \frac{\partial \rho_S}{\partial \rho_p} - G_{\rho S} \rho \rho_S^2. \quad (\text{A9}) \end{aligned}$$

The symmetry energy is half the second derivative in symmetric matter with  $p_F = p_{Fp} = p_{Fn}$

$$\frac{1}{2} \frac{\partial^2 f}{\partial \delta^2} \Big|_{\delta=0} = \frac{p_F^2}{6\sqrt{p_F^2 + m^2}} - \frac{G_{\rho S} \rho \rho_S^2}{2}. \quad (\text{A10})$$

- 
- [1] B. A. Li, Phys. Rev. Lett. **85**, 4221 (2000); ibid. **88**, 192701 (2002).
  - [2] B. A. Li, L. W. Chen and C. M. Ko, Phys. Rep. **464**, 113 (2008).
  - [3] J. M. Lattimer and M. Prakash, Phys. Rep. **333**, 121 (2000); Science **304**, 536 (2004).
  - [4] J. M. Lattimer and A. W. Steiner, Eur. Phys. J. A **50**, 40 (2014).
  - [5] B. A. Li and X. Han, Phys. Lett. B **727**, 276 (2013).
  - [6] L. W. Chen, Nucl. Phys. Rev. **31**, 273 (2014).
  - [7] M. B. Tsang, Yingxun Zhang, P. Danielewicz, M. Famiano, Zhuxia Li, W. G. Lynch and A. W. Steiner, Phys. Rev. Lett. **102**, 122701 (2009); ibid., Int. J. Mod. Phys. E **19**, 1631 (2010).
  - [8] J. M. Lattimer and Y. Lim, Astrophys. J. **771**, 51 (2013).
  - [9] N. Wang, M. Liu, L. Ou and Y. Zhang, Phys. Lett. B **751**, 553 (2015).
  - [10] B. A. Li, W. J. Guo and Z. Z. Shi, Phys. Rev. C **91**, 044601 (2015).
  - [11] Y. J. Wang and C. C. Guo, et al., Eur. Phys. J. A **51**, 37 (2015).
  - [12] W. J. Xie, Z. Q. Feng, J. Su, F. S. Zhang, Phys. Rev. C **91**, 054609 (2015).
  - [13] B. A. Brown, Phys. Rev. Lett. **85**, 5296 (2000).
  - [14] L. W. Chen, C. M. Ko, B. A. Li, Phys. Rev. C **72**, 064309 (2005).
  - [15] C. Fuchs, H. H. Wolter, Eur. Phys. J. A **30**, 5 (2006).
  - [16] C. J. Horowitz and J. Piekarewicz, Phys. Rev. Lett. **86**, 5647 (2001).
  - [17] W. Z. Jiang, B. A. Li, and L. W. Chen, Phys. Lett. B **653**, 184 (2007).
  - [18] L. W. Chen, C. M. Ko and B. A. Li, Phys. Rev. C **76**, 054316 (2007).
  - [19] Z. Xiao, B. A. Li and L. W. Chen, G. C. Yong, M. Zhang, Phys. Rev. Lett. **102**, 062502 (2009).
  - [20] P. Russotto, W. Trautmann, Q. F. Li et al., Phys. Lett. B **697**, 471 (2011).
  - [21] Z. Q. Feng and G. J. Ming, Phys. Lett. B **683**, 140-144 (2010).
  - [22] Z. G. Xiao, G. C. Yong, L. W. Chen, B. A. Li, et al., Eur. Phys. J. A **50**, 37 (2014).
  - [23] H. Lenske and C. Fuchs, Phys. Lett. B **345**, 355 (1995).
  - [24] B. A. Nikolaus, T. Hoch, and D. G. Madland, Phys. Rev. C **46**, 1757 (1992).
  - [25] T. Burvenich, D. G. Madland, J. A. Maruhn, and P. G. Reinhard, Phys. Rev. C **65**, 044308 (2002).
  - [26] P. Finelli, N. Kaiser, D. Vretenar, and W. Weise, Nucl. Phys. A **435**, 449 (2004).
  - [27] J. N. Ginocchio, Phys. Rep. **315**, 231 (1999).
  - [28] H. Liang, J. Meng, and S. G. Zhou, Phys. Rep. **570**, 1 (2015).
  - [29] R. Y. Yang, W. Z. Jiang, Q. F. Xiang, D. R. Zhang, S. N. Wei, Eur. Phys. J. A **50**, 188 (2014).
  - [30] J. R. Shepard, J. A. McNeil and S. J. Wallace Phys. Rev. Lett. **50**, 1443 (1983).
  - [31] B. C. Clark and S. Hama, Phys. Rev. Lett. **50**, 1644 (1983).
  - [32] J. D. Walecka, Ann. Phys. (NY) **83**, 491 (1974).
  - [33] J. Boguta and A. R. Bodmer, Nucl. Phys. A **292**, 423 (1977).
  - [34] S. A. Chin, Ann. Phys. **108**, 301 (1977).

- [35] B. D. Serot and J. D. Walecka, *Adv. Nucl. Phys.* **16**, 1 (1986).
- [36] P. G. Reinhard, *Rep. Prog. Phys.* **52**, 439 (1989).
- [37] P. Ring, *Prog. Part. Nucl. Phys.* **37**, 193 (1996).
- [38] B. D. Serot and J. D. Walecka, *Int. J. Mod. Phys. E* **6**, 515 (1997).
- [39] M. Bender, P. H. Heenen, and P. G. Reinhard, *Rev. Mod. Phys.* **75**, 121 (2003).
- [40] J. Meng, H. Toki, S. G. Zhou, S. Q. Zhang, W. H. Long, and L. S. Geng, *Prog. Part. Nucl. Phys.* **57**, 470 (2006).
- [41] W. Z. Jiang, B. A. Li, and L. W. Chen, *Phys. Rev. C* **76**, 054314 (2007).
- [42] M. Dutra, O. Lourenco, S.S. Avancini, B.V. Carlson, A. Delfino, et. al., *Phys. Rev. C* **90**, 055203 (2014).
- [43] J. Margueron, J. Navarro and N. V. Giai, *Phys. Rev. C* **66**, 014303 (2002).
- [44] P. Bedaque and A. W. Steiner, *Phys. Rev. Lett.* **114**, 031103 (2015).
- [45] S. Weinberg, *Physica A* **96**, 327 (1979).
- [46] S. Weinberg, *Nucl. Phys. B* **363**, 3 (1991).
- [47] Y. Nambu, G. J. Lasinio, *Phys. Rev.* **122**, 345 (1961).
- [48] M. Gell-Mann, M. Levy, *Nuovo Cimento* **16**, 705 (1960).
- [49] J. Boguta, *Phys. Lett. B* **120**, 34 (1983).
- [50] R. J. Furnstahl and B. D. Serot, *Phys. Rev. C* **47**, 2338 (1993).
- [51] A. Lacour, J.A. Oller, U.-G. Meissner, *Ann. Phys.* **326**, 241 (2011).
- [52] S. P. Klevansky, *Rev. Mod. Phys.* **64**, 649 (1992).
- [53] U. Vogl and W. Weise, *Prog. Part. Nucl. Phys.* **27**, 195 (1991).
- [54] M. Buballa, *Phys. Rept.* **407**, 205 (2005).
- [55] W. Bentz and A. W. Thomas, *Nucl. Phys. A* **696**, 138 (2001).
- [56] V. Koch, T. S. Biro, J. Kunz and U. Mosel, *Phys. Lett. B* **185**, 1 (1987).
- [57] I. N. Mishustin, L. M. Satarov and W. Greiner, *Phys. Rep.* **391**, 363 (2004).
- [58] S. T. Uechi and H. Uechi, *arXiv:1007.3630 [nucl-th]*.
- [59] C. Providencia, J. M. Moreira, J. da Providencia, and S. A. Moszkowski, *AIP Conf. Proc.* **660**, 231 (2003).
- [60] Y. Tsue, J. da Providencia, C. Providencia, M. Yamamura, *Prog. Theor. Phys.* **123**, 1013 (2010).
- [61] T.-G. Lee, Y. Tsue, J. da Providencia, C. Providencia, M. Yamamura, *Prog. Theor. Exper. Phys.* **2013**, 013D02 (2013).
- [62] P. Demorest, T. Pennucci, S. Ransom, M. Roberts and J. Hessels, *Nature* **467**, 1081(2010).
- [63] J. Antoniadis, P. C. Freire, N. Wex, T. MTauris, R. S. Lynch, et.al., *Science* **340**, 1233232 (2013).
- [64] W. Z. Jiang, B. A. Li, F. J. Fattoyev, *Eur. Phys. J. A* **51**, 119 (2015).
- [65] S. Guillot and R. E. Rutledge, *Astrophys. J.* **796**, 1, (2014).
- [66] A. W. Steiner, J. M. Lattimer, E. F. Brown, *Astrophys. J.* **765**, L5 (2013).
- [67] S. Bogdanov, *Astrophys. J.* **762**, 96 (2013).
- [68] J. Poutanen, J. Nättilä, J. J. E. Kajava, et. al., *Mon. Not. Roy. Astron. Soc.* **442**, 3777 (2014).
- [69] C. O. Heinke, H. N. Cohn, P. M. Lugger, N. A. Webb, W. C. G. Ho, et. al., *Mon. Not. Roy. Astron. Soc.* **444**, 443 (2014).
- [70] J. M. Lattimer and A. W. Steiner, *Astrophys. J.* **784**, 123 (2014).
- [71] F. Özel, D. Psaltis, T. Güver, G. Baym, C. Heinke, and S. Guillot, *arXiv:1505.05155*.
- [72] M. C. Miller, *arXiv/1312.0029*.
- [73] P. Haensel, *Astron. Astrophys.* **380**, 186 (2001).
- [74] C. M. Zhang, H. X. Yin, Y. Kojima, H. K. Chang, et.al., *Mon. Not. Roy. Astron. Soc.* **374**, 232 (2007).
- [75] V. Suleimanov, J. Poutanen, M. Revnivtsev, and K. Werner, *Astrophys. J.* **742**, 122 (2011).
- [76] K. Hagivara, et.al, Particle Data Group, *Phys. Rev. D* **66**, 010001 (2002).
- [77] G.A. Lalazissis, J. König, and P. Ring, *Phys. Rev. C* **55**, 540 (1997).
- [78] R. B. Wiringa, V. Fiks, A. Fabrocini, *Phys. Rev. C* **38**, 1010 (1988).
- [79] A. Szmajlinski, W. Wojcik, M. Kutschera, *Acta Phys. Polon. B* **37**, 277 (2006).
- [80] M. Dutra, O. Lourenco, J.S. Sa Martins, A. Delfino, J.R. Stone, P.D. Stevenson, *Phys. Rev. C* **85**, 035201 (2012).
- [81] D. H. Wen, B. A. Li, and L. W. Chen, *Phys. Rev. Lett.* **103**, 211102 (2009).
- [82] J. Oppenheimer and G. Volkoff, *Phys. Rev.* **55**, 374 (1939).
- [83] R. C. Tolman, *Phys. Rev.* **55**, 364 (1939).
- [84] G. Baym, C. Pethick and P. Sutherland, *Astrophys. J.* **170**, 299 (1971).
- [85] K. Iida and K. Sato, *Astrophys. J.* **477**, 294 (1997).
- [86] M. Bigdeli and S. Elyasi, *Eur. Phys. J. A* **51**, 38 (2015).
- [87] J. M. Lattimer and M. Prakash, *Phys. Rep.* **442**, 109 (2007).
- [88] J.M. Lattimer, M. Prakash, *Astrophys. J.* **550**, 426 (2001).
- [89] B. A. Li and A. W. Steiner, *Phys. Lett. B* **642**, 436 (2006).